INTERNATIONAL JOURNAL FOR NUMERICAL METHODS IN FLUIDS
Int. J. Numer. Meth. Fluids 2002; **40**:313–322 (DOI: 10.1002/fld.288)

On 'spurious' eddies

D. Drikakis[1,*], L. G. Margolin[2] and P. K. Smolarkiewicz[3]

[1]*Engineering Department, Queen Mary, University of London, London E1 4NS, U.K.*
[2]*Center for Nonlinear Science, Los Alamos National Laboratory, Los Alamos, NM 87545, U.S.A.*
[3]*National Center for Atmospheric Research, Boulder, CO 80307, U.S.A.*

SUMMARY

Recently, several papers have appeared in the CFD literature, proposing an idealized instability problem as a benchmark for discriminating among numerical algorithms for two-dimensional Navier–Stokes flows. The problem is a double shear layer simulated at coarse resolution and with a prescribed interface perturbation. A variety of second-order accurate schemes have been tested, with all results falling into one of two solution patterns—one pattern with two eddies and the other with three eddies. In the literature, there is no fast-and-firm rule to predict the results of any particular algorithm. However, it is asserted that the two-eddy solution is correct. Our own research has led to two conclusions. First, the appearance of the third eddy is tied up with small details of the truncation error; we illustrate this point by prescribing small changes that lead to reversal of the appearance/disappearance of the third eddy in several schemes. Second, we discuss the realizability of the two solutions and suggest that the three-eddy solution is the more physical. Overall, we conclude that this problem is a poor choice of benchmark to discriminate among numerical algorithms. Copyright © 2002 John Wiley & Sons, Ltd.

KEY WORDS: unsteady flows; vortices; high-resolution methods

1. INTRODUCTION

We investigate the formation of spurious vortical structures in time-dependent simulations of incompressible flow. Our work is motivated by previous studies (Reference [1], and the references therein) that have documented the formation of 'spurious eddies' in coarsely resolved simulations of 2D vortex-street flows. In general, we seek an understanding and control of the numerical mechanisms that underlie the formation of these spurious structures. Our study demonstrates the sensitivity of the simulated behaviour of flows to the numerical discretization of the advective terms, especially when vorticity dynamics plays an essential role in flow evolution. This sensitivity is of particular relevance to large-eddy simulation (LES) of turbulent flows. In LES, the advective term discretization can alter the simulated large-eddy

*Correspondence to: D. Drikakis, Department of Engineering, Queen Mary College, University of London, London E1 4NS, U.K.

Contract/grant sponsor: US Department of Energy;
Contract/grant sponsor: National science foundation

Received May 2001
Revised October 2001

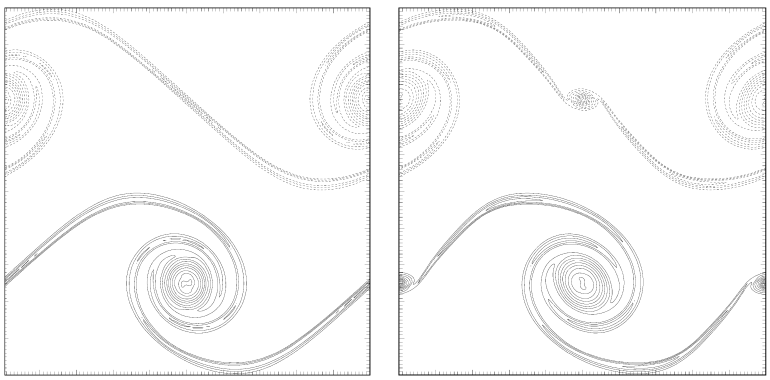

Figure 1. Vorticity isolines for correct (left) and spurious (right) solutions. Negative values are dashed.

structures and subsequently overwhelm the effects of unresolved scales estimated by a subgrid scale model. An understanding of these issues will lead to better algorithms, including the consistent design of spatio-temporal filters and subgrid scale models.

The modelled flow is the evolution of a double shear-layer on a doubly periodic domain, governed by the incompressible Navier–Stokes equations

$$\begin{aligned} \frac{\partial u_i}{\partial x_i} &= 0 \\ \frac{\partial u_i}{\partial t} + \frac{\partial u_i u_j}{\partial x_j} &= -\frac{\partial p}{\partial x_i} + \frac{1}{Re}\Delta u_i \end{aligned} \tag{1}$$

where u_i ($i = 1, 2$ refers to the space co-ordinates x, y) are the velocity components, p is the pressure, Re is the Reynolds number, and t is the time; all variables are non-dimensionalized. With δ determining the shear layer thickness, the initial condition

$$u = \begin{cases} \tanh((y - 0.25)\delta) & \text{if } y \leqslant 0.5 \\ \tanh((0.75 - y)\delta) & \text{if } y > 0.5 \end{cases} \tag{2}$$

results in hydrodynamically unstable flow, and so one may expect different flow realizations depending on the details of the initial perturbation. Although we specify only the excitation of the primary mode (i.e. wavenumber one),[†] the truncation error of the numerical scheme presents an additional perturbation, whose magnitude depends on the resolution length scale. For a fixed Reynolds number and for all considered numerical algorithms, this problem has the converged solution[‡] of a regular vortex street (cf. left panel in Figure 1). At coarse resolutions, some algorithms evince a spurious eddy embedded between the two primary vortices (e.g. right panel in Figure 1), the apparent result of a wavenumber two perturbation.

[†]Following [1], we consider a small sinusoidal perturbation of the initial spanwise velocity, $v = v' \sin(2\pi x)$.
[‡]The details of this convergence depend both on the Reynolds number and the advective scheme employed.

The converged solution is most likely a metastable mathematical peculiarity unrealizable in nature.[§] Nonetheless, the task of isolating the precise characteristics of the schemes that lead to the spurious eddies is an interesting challenge.

We have performed hundreds of numerical experiments using various Godunov methods [2], and various non-oscillatory forward-in-time (NFT) semi-Lagrangian/Eulerian schemes [3]. Our experiments identify no simple, single explanation for the formation of the spurious eddy valid for all the tested schemes. The only universal conclusion is that the generation of spurious eddies is tied to fine details of the truncation error. For example, depending on the detailed form of the Godunov flux spurious eddies may or may not appear. In the class of NFT schemes, those based on semi-Lagrangian (i.e. trajectory) integrals tend to produce 'correct' solutions, whereas Eulerian (i.e. control volume) integrals tend to exhibit the spurious eddy.[¶]

We will employ a heuristic analysis of the vorticity equation implied by the discretized momentum equations, and identify unphysical forcings originating in the truncation error terms. We conjecture that these numerical forcings are responsible for the spurious eddies. To verify this hypothesis, we develop modifications of upwind methods and demonstrate their effectiveness in eliminating the spurious eddies.

The paper is organized as follows. In Section 2, we outline the numerical methods employed. In Section 3, we summarize the solutions obtained with different methods. In Section 4, we present a vorticity argument that aims at explaining the formation of spurious solutions, and propose remedies for suppressing the spurious eddies. Remarks in Section 5 conclude the paper.

2. NUMERICAL METHODS

2.1. Godunov-type methods

To take full advantage of the Godunov methods designed for hyperbolic conservation laws, the incompressible equations (1) are cast in a compressible format by means of artificial-compressibility, where at each instant t, the augmented pseudocompressible system

$$\begin{aligned} \frac{1}{\beta}\frac{\partial p}{\partial \tau} + \frac{\partial u_i}{\partial x_i} &= 0 \\ \frac{\partial u_i}{\partial \tau} + \frac{\partial}{\partial x_j}(u_i u_j + p\delta_{ij}) &= -\alpha(u_i - \tilde{u}_i) + \frac{1}{Re}\Delta u_i \end{aligned} \tag{3}$$

is integrated in a pseudotime τ to a steady state, assuming an artificial speed of sound $\sqrt{\beta}$ ($\beta \equiv 1$ in this study). Here, $\tilde{u}_i$ denotes the solution at the instant t, whereas all tilde-free variables are allowed (in principle) to vary in the pseudotime $\tau \in [t, t + \Delta t]$. The attenuation forcing on the right-hand side (rhs) of the momentum equation damps the flow divergence to zero (given $\partial \tilde{u}_i/\partial x_i = 0$) at the rate $\alpha \equiv (\Delta t)^{-1}$. In the steady state at $\tau = t + \Delta t$, all $\partial/\partial\tau$ terms vanish and the damping term on the rhs becomes $\partial u_i/\partial t$, i.e. the u_i solution becomes

[§] For a solenoidal white-noise initial perturbation, our experiments showed that all solutions evince the secondary eddy for all methods considered in this study.

[¶] Thus, not all upwind-biased dissipative methods result in spurious vortices!

the $\tilde{u}_i$ solution at $t + \Delta t$. The default time integration with respect to τ employs a fourth-order Runge–Kutta scheme, while a non-linear multigrid method is used to accelerate the convergence toward the steady state.[||] The viscous terms are discretized by standard central differences. The reader interested in further details is referred to [2, 4] and the references therein.

In all Godunov methods considered in this study, the advective flux derivatives on the lhs of (3) are discretized at the centre of the control volume using the values of the intercell fluxes:

$$E_{i+1/2} = \tfrac{1}{2}(E_{\mathrm{L}} + E_{\mathrm{R}}) - \tfrac{1}{2}|A|(U_{\mathrm{R}} - U_{\mathrm{L}}) \tag{4}$$

where A approximates $\partial E/\partial U$ (the entries of the Jacoby matrix), E is the x-direction advective flux

$$E \equiv \begin{pmatrix} u \\ u^2 + p \\ uv \end{pmatrix} \tag{5}$$

and $E_{\mathrm{L}} = E_{\mathrm{L}}(U_{\mathrm{L}})$ and $E_{\mathrm{R}} = E_{\mathrm{R}}(U_{\mathrm{R}})$ denote the left and right states of the flux, respectively, at the cell face of the computational volume. Similarly, U_{L} and U_{R} are the left and right states, respectively, of the vector of the primitive variables $U = (p, u, v)^{\mathrm{T}}$ at the cell face of the computational volume. The second term in the rhs of (4) is the wave-speed-dependent term (WST).

The definition of the intercell flux function distinguishes the different Godunov schemes implemented in this study; these schemes are the Rusanov, Lax–Friedrichs (LF), Einfeldt's variant of Harten–Lax–van Leer (HLLE), Toro's first-order centred (FORCE) (details of these schemes can be found in [5]) and uniformly high-order (UHO) characteristic based [2]. All listed Godunov schemes require calculating the left and right states of the primitive variables at the cell faces. Here, two interpolation schemes have been employed: (a) the 'third-order' Lagrangian interpolator [6]; and (b) the MUSCL scheme [7]. For a comprehensive review of the listed schemes, see [8].

2.2. NFT approach

Our basic NFT approach for approximating integrals of the governing equations of motion (1) on a discrete mesh is second-order accurate in space and time. The two optional model algorithms, Eulerian and semi-Lagrangian, correspond to the point-wise and trajectory-wise integrals of the mathematically equivalent evolution equations (1) and

$$\frac{\mathrm{D}u_i}{\mathrm{D}t} = -\frac{\partial p}{\partial x_i} + \frac{1}{Re}\nabla u_i \tag{6}$$

respectively, $\mathrm{D}/\mathrm{D}t$ denotes the material derivative.

[||]Sensitivity tests using various time-stepping schemes both with and without the multigrid accelerator shows that the formation of spurious vortices depends principally on the advective scheme employed. In particular, β has no effect on the occurrence of spurious eddies, but does affect the convergence rate of the multigrid accelerator.

We assume all variables are co-located—a choice important for the efficacy of the unified semi-Lagrangian/Eulerian NFT approach [3]—and write the resulting finite-difference approximations in the compact form

$$\boldsymbol{\psi}_{\mathbf{i}}^{n+1} = \mathrm{LE}_{\mathbf{i}}(\tilde{\boldsymbol{\psi}}) + 0.5\Delta t \mathbf{F}_{\mathbf{i}}^{n+1} \tag{7}$$

Here, the indices $\mathbf{i}$ and n denote the spatial and temporal location on a (logically) rectangular Cartesian mesh; LE denotes either an advective semi-Lagrangian or a flux-form Eulerian NFT transport operator (Sections 3.1 and 3.2 in [3], respectively);** $\tilde{\boldsymbol{\psi}} \equiv \boldsymbol{\psi}^n + 0.5\Delta t \mathbf{F}^n$. Transporting the auxiliary field $\tilde{\boldsymbol{\psi}}$ (rather than the fluid variable alone) has been shown to be important for maintaining the second-order accuracy and the stability of forward-in-time approximations [10]. In the Eulerian algorithm, transporting $\tilde{\boldsymbol{\psi}}$ is a consequence of compensating the first-order truncation error proportional to the divergence of the advective flux of the rhs of the evolution equations, while in the semi-Lagrangian algorithm it derives straightforwardly from the trapezoidal-rule approximation for the integral on the rhs; see References [3, 9], for further discussions.

Completion of the model algorithm requires formulating the boundary value problem for pressure implied by the mass continuity constraint $\nabla \cdot \mathbf{u} = 0$. In [3], we have outlined the essential steps of this fairly standard projection procedure. The resulting elliptic equation is solved, subject to appropriate boundary conditions, using a pre-conditioned non-symmetric Krylov solver.

3. RESULTS

We have used the algorithms outlined in the preceding section on both the 'coarse' (128×128) and the 'fine' (256×256) grid; selected computations were also performed on a 512×512 grid. Together this has led to a large series of numerical experiments gathering systematic evidence about the response of various schemes. All experiments assumed the Reynolds number $Re = 10\,000$ in (1), the thickness of the shear layer $\delta = 100$ in (2), and the amplitude of the initial span-wise perturbation $v' = 0.05$. Depending on the Reynolds number and the thickness of the shear layer spurious vortices may or may not appear on coarser grids. The larger the Re or δ, the more likely is the occurrence of the spurious solutions. Here, we consider a relatively thin layer to emphasize the development of the spurious eddies. With the given set of parameters, all analysed schemes converge to the correct solution, as evidenced by the fine-grid solutions. We summarize our results below and, for the reader's convenience, collect the most representative experiments in Tables I and II.

For Godunov schemes there is no obvious categorization determining whether the third eddy appears. In particular, the Rusanov (RU), LF, and HLLE schemes do not evince spurious eddies even on the coarse grid. Although the FORCE schemes have substantial similarities to RU and LF—none of them requires solving the Riemann problem, and they all qualify as centred schemes—some variants of FORCE exhibit spurious eddy and some do

**Both operators employ multidimensional positive definite advection transport algorithm (MPDATA) schemes [9] and preserve sign or monotonicity of the transported variables.

Table I. Spurious eddy experiments using Godunov schemes.

Scheme	128×128	256×256
RU	Correct	Correct
UHO	Spurious	Correct
LF	Correct	Correct
FORCE	Spurious	Correct
FORCE^2	Correct	Correct
HLLE	Correct	Correct

Table II. Spurious eddy experiments using NFT schemes.

Scheme	128×128	256×256
SL	Correct	Correct
SL-FCT	Correct	Correct
SL-SMG	Correct	Correct
SL-1	Spurious	Spurious
EU	Spurious	Correct
EU-CMP	Correct	Correct
EU-TRS	Correct	Correct

not.[††] Interestingly, the FORCE schemes that use higher-order interpolation (and so are less diffusive than the equivalent schemes with the first-order interpolation) evince no spurious eddies. In general, the appearance of the spurious eddy does not depend on whether the 'third-order' Lagrangian or MUSCL interpolation is employed in a Godunov-type method; higher-order interpolation of the Godunov flux also has no direct impact on the occurrence of the spurious eddies. For example, the third-order version of the UHO results in spurious vortices despite the higher accuracy of interpolation.

For standard second-order NFT schemes there is a categorization based on flux-form versus advective form. The latter (i.e. semi-Lagrangian; SL in Table II) do not produce the spurious eddy, while the former (i.e. Eulerian; EU in Table II) do. However, altering fine details of the truncation errors may reverse either of these results. For instance, increasing the dissipation of semi-Lagrangian schemes with flux-corrected-transport (SL-FCT) or with a Smagorinsky subgrid-scale turbulence model (SL-SMG), does not alter the correct solution. In contrast, the use of some first-order upwinding inside the LE transport operator leads to spurious solutions (SL-1). For Eulerian schemes, a noticeable sensitivity is to the definition of the advective (as opposed to advected) velocity. For instance, replacing the explicit evaluation of advective velocities at cell faces via arithmetic average with a compact average (i.e. implicit in space;

[††]In Table I, the two variants of the FORCE scheme differ in details of implementation of higher-order interpolation [8].

EU-CMP), or with a weighted average over a broader (transverse) stencil (EU-TRS), may eliminate or retard substantially the growth of the third eddy.

We conclude that the results depend on details of the non-linear truncation error that, in turn, depends on the discretization of the momentum flux. In the next section, we will employ a heuristic analysis of the vorticity equation implied by the discretized momentum equations of a generic upwind scheme, and identify unphysical terms originating from the truncation error. We conjecture that these terms control the appearance of the spurious eddies. To verify this hypothesis, we develop customized modifications of higher-order upwind methods and verify their effectiveness in eliminating the spurious eddies.

4. VORTICITY ARGUMENT AND NUMERICAL MODIFICATIONS

Let us consider the inviscid system in (1). Using an explicit discretization in time while retaining a continuous representation in space, keeping track separately of the advective and advected velocities, and applying $\nabla\times$ to the resulting idealized algorithm leads to the vorticity equation (cf. [8])

$$\frac{\omega^{n+1}-\omega^n}{\Delta t}+\tilde{\mathbf{u}}\cdot\nabla\omega=(\tilde{u}_x u_y-u_x\tilde{u}_y)+(\tilde{v}_x v_y-v_x\tilde{v}_y) \tag{8}$$

where $\tilde{u}$ and $\tilde{v}$ identify the advective velocities. Analytically, $\tilde{\mathbf{u}}=\mathbf{u}$ so the rhs of (8) vanishes identically, leaving the correct time-discretized vorticity equation for ideal two-dimensional flows. In discrete models, however, $\tilde{\mathbf{u}}\neq\mathbf{u}$ in general, and the two terms on the rhs of (8) do not vanish. Typically, $\tilde{\mathbf{u}}=\mathbf{u}+\mathcal{O}(\Delta x^2)$, and the artificial vorticity forcing appears at the second order.

Fully third-order-accurate discretizations may suppress the forcing on the rhs of (8). However, such approximations are not easy to develop for control-volume non-oscillatory schemes. There are variants of MPDATA that converge at the third order [11], given a uniform advective flow. For variable flows these schemes are still second-order accurate, and they do evince the spurious eddy in the problem at hand. However, combining these with a compact definition of the advective velocity sufficiently reduces the magnitude of the rhs of (8), and allows Eulerian MPDATA to recover the two-eddy solution.

Equation (8) by no means implies that suppressing the source necessarily requires a fully third-order accurate discretization of the momentum equation in (1). Favourable cancellations can effectively reduce the amplitude of the forcing at the second order, as is illustrated by our results summarized in the preceding section. For simple algorithms such as standard centred differences, it is feasible to derive the finite-difference vorticity equation implied by the discrete momentum equation, and to reveal the explicit form of the rhs of (8). In the case of complicated algorithms like Godunov- or NFT-type methods this seems a hopeless task. However, some insights have been gained by pursuing heuristic vorticity arguments for the general form of the Godunov flux [8].

The Godunov flux, or a generic upwind scheme flux, may be viewed as the sum of a nondissipative centred-in-space finite-difference approximation to the momentum flux and a Fickian flux of the primitive variables with a diffusion coefficient dependent on the flow. In the implied vorticity equation, similar to an eddy viscosity, the Fickian flux engenders two types of terms: equivalent Fickian fluxes of the vorticity and solenoidal-type fluxes that depend on

various products of spatial derivatives of flow variables. Following this notion, the originally deficient (spurious-eddies-wise) FORCE and UHO schemes have been modified such as to accentuate benefits of the Fickian flux and diminish the magnitude of the eventual 'baroclinic' source. Technically, this is achieved by using low-order interpolation in the WST of (4); [8]. The modified schemes produce the correct solution while adding only small extra dissipation as measured by diverse benchmark tests.

5. REMARKS

Our extensive experience with hundreds of simulations has led us to three general propositions. First, from the perspective of numerical analysis, an understanding of the occurrence of the spurious eddy is buried in the details of the truncation error. In particular, it appears that the lack of proper tensor invariance of the error (i.e. dependence on mesh orientation) is more important than its magnitude. This is why the flux-form schemes are more susceptible to the third eddy. Second, from a phenomenological view point, there are two apparent mechanisms of controlling the growth of the spurious eddy—either accelerating the roll-up of the primary eddy or diffusing the vorticity of the secondary eddy. This explains why the spurious eddy can be controlled by either increasing or decreasing dissipation intelligently. Third, from the applications view point, the absence of the spurious eddy is not tantamount to an accurate solution. Detailed comparisons of the vorticity fields and the dissipation histories show that standard semi-Lagrangian NFT schemes are not necessarily more accurate than their Eulerian counterparts (see also [3] for additional comparisons). In fact, the Eulerian schemes appear more accurate as they follow a dissipation path consistent with highly resolved calculations. Thus, while the 'spurious-eddy' test promotes understanding of an individual method, it is not a discriminating benchmark for assessing that method's performance in under-resolved simulations.

The essence of the propositions is illustrated in Figures 2, and 3. Figure 2 shows late-time solutions from high-resolution simulations on 512×512 grid using an Eulerian (left panel) and semi-Lagrangian (right panel) NFT schemes.[‡‡] Comparing the centres of the eddies in both panels shows that the semi-Lagrangian solution rolls up slightly faster. At lower resolution both solutions roll up slower, but the difference between the Eulerian and semi-Lagrangian result is more pronounced, and the Eulerian scheme exhibits a tendency for the third eddy (cf. Figure 1 for coarser solutions on 256×256 grid at much earlier time). On even coarser grids the core of the primary eddy is unresolved and there is not sufficient detail to judge which eddy rolls faster. Figure 3 displays the dissipation histories, corresponding to the simulations depicted in Figure 2. Solid lines are for the negative of the total kinetic energy decay rate $-\partial\langle e\rangle/\partial t$, and dashed lines are for the negative of the viscous dissipation $-\langle Re^{-1}\mathbf{u}\Delta\mathbf{u}\rangle$; where $\langle\,\rangle$ denotes the domain mean integral value, and e is the kinetic energy. For the Eulerian solution, the effective decay rate is uniformly larger than the viscous dissipation, documenting the weak implicit dissipation of the numerical approximation. This is not the case for the semi-Lagrangian solution, which first generates energy, and then later dissipates it at an increased rate. The unphysical 'kink' in the semi-Lagrangian solution appears dramatically accentuated

[‡‡]Both panels use the same interval to contour vorticity field.

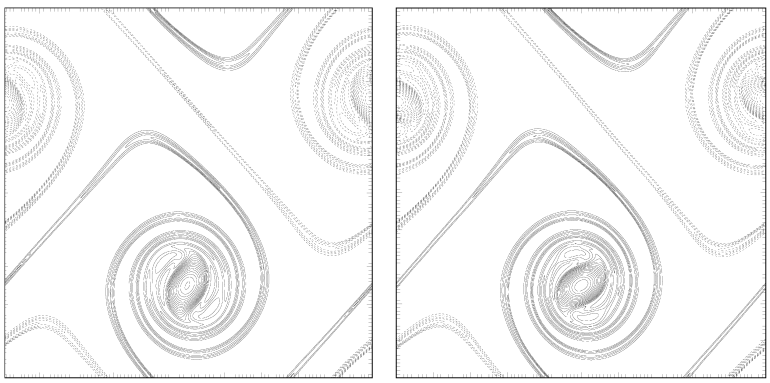

Figure 2. Vorticity isolines for Eulerian (left) and semi-Lagrangian (right) solutions. Negative valuesare dashed.

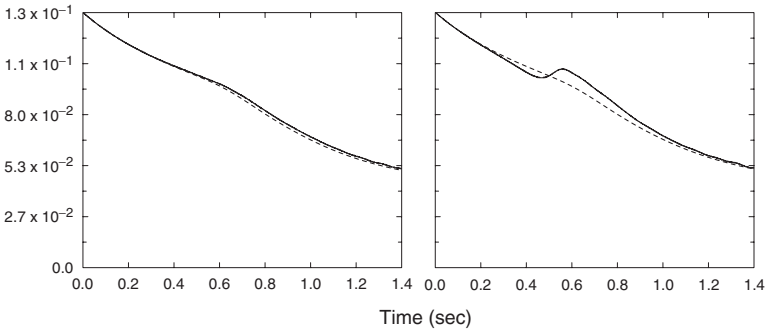

Figure 3. Dissipation histories for the solutions in Figure 2. Kinetic energy decay rate (solid lines) vs viscous dissipation (dashed lines).

in coarser resolutions, although the solution remains free of the third eddy. The coarsely resolved Eulerian scheme in contrast evinces the third eddy, while maintaining an energy dissipation path consistent with the more resolved solution.

ACKNOWLEDGEMENTS

Helpful discussions with William Rider are gratefully acknowledged. Los Alamos National Laboratory is operated by the University of California for the U.S. Department of Energy. National Center for Atmospheric Research is sponsored by the National Science Foundation. LGM and PKS were supported in part by the US Department of Energy 'Climate Change Prediction Program' in this research.

REFERENCES

1. Minion ML, Brown DL. Performance of under-resolved two-dimensional incompressible flow simulations II. *Journal of Computational Physics* 1997; **138**:734–765.
2. Drikakis D. Uniformly high order methods for unsteady incompressible flows. In *Godunov Methods*:*Theory and Applications*, Toro EF (ed.). Kluwer Plenum Academic: Dordrecht, 2001; 263–283.

3. Smolarkiewicz PK, Margolin LG. On forward-in-time differencing for fluids: an Eulerian/semi-Lagrangian nonhydrostatic model for stratified flows. *Atmospheric Ocean Special* 1997; **35**:127–152.
4. Drikakis D, Iliev O, Vassileva DP. A nonlinear multigrid method for the three-dimensional incompressible Navier–Stokes equations. *Journal of Computational Physics* 1998; **146**:301–321.
5. Toro EF. *Riemann Solvers and Numerical Methods for Fluid Dynamics*. Springer: Berlin, 1999.
6. Drikakis D, Govatsos P, Papantonis D. A characteristic-based method for incompressible flows. *International Journal for Numerical Methods in Fluids* 1994; **19**:667–685.
7. Van Leer B. Towards the ultimate conservative difference scheme V. Second-order sequel to Godunov's method. *Journal of Computational Physics* 1979; **32**:101–136.
8. Drikakis D, Smolarkiewicz PK. On spurious vortical structures. *Journal of Computational Physics* 2001; **172**: 309–325.
9. Smolarkiewicz PK, Margolin LG. MPDATA: a finite-difference solver for geophysical flows. *Journal of Computational Physics* 1998; **140**:459–480.
10. Smolarkiewicz PK, Margolin LG. On forward-in-time differencing for fluids: Extension to a curvilinear framework. *Monthly Weather Review* 1993; **121**:1847–1859.
11. Margolin LG, Smolarkiewicz PK. Antidiffusive velocities for multipass donor cell advection. *SIAM Journal on Scientific Computing* 1998; **20**(3):907–929.

